

Study of errors in strong gravitational lensing

Thomas P. Kling
tkling@bridgew.edu

Department of Physics, Bridgewater State College, Bridgewater, MA 02325

Simonetta Frittelli

Department of Physics, Duquesne University, Pittsburgh, PA 15282

ABSTRACT

We examine the accuracy of strong gravitational lensing determinations of the mass of galaxy clusters by comparing the conventional approach with the numerical integration of the fully relativistic null geodesic equations in the case of weak gravitational perturbations on Robertson-Walker metrics. In particular, we study spherically-symmetric, three-dimensional singular isothermal sphere models and the three-dimensional matter distribution of Navarro et al. (1997), which are both commonly used in gravitational lensing studies. In both cases we study two different methods for mass-density truncation along the line of sight: hard truncation and conventional (no truncation). We find that the relative error introduced in the total mass by the thin lens approximation alone is less than 0.3% in the singular isothermal sphere model, and less than 2% in the model of Navarro et al. (1997). The removal of hard truncation introduces an additional error of the same order of magnitude in the best case, and up to an order of magnitude larger in the worst case studied. Our results ensure that the future generation of precision cosmology experiments based on lensing studies will not require the removal of the thin-lens assumption, but they may require a careful handling of truncation.

Subject headings: gravitational lensing — galaxies: clusters:

1. Introduction

In the current age of precision cosmology, the fundamental parameters of the favored cosmological model can be measured with high accuracy. Strong and weak gravitational lensing studies are particularly important in this endeavor as an independent and relatively assumption-free measure of mass morphology in clusters of galaxies.

Conventional gravitational lensing studies continue to utilize the standard assumption of thin lenses. This allows for the actual path of photons from source to observer to be approximated by its asymptotics, with a sharp bending at the plane where the lens is located. There is, clearly, some error involved in this approximation, but the size of this error has not been rigorously examined, to our knowledge.

A question that will be important as the accuracy increases is at what point the error in the conventional approach becomes comparable to the uncertainty in the cosmological parameters. At that point, accurate modeling of lensing events will require a more accurate version of the lens equation, or an efficient algorithm to calculate the photon paths. In this respect, seminal proposals that improve on the conventional approach exist, dating from the 1990's. In the work of Pyne & Birkenshaw (1993), higher-order lens equations in cosmological backgrounds are developed. A different style of approximation which correctly utilizes the thin-lens paths as the zeroth-order path is introduced in Kling et al (2000, 2001).

The same motivation sparked some interest in revisiting the foundations of gravitational lensing

theory with the aim of developing the concept of the lens equation without reference to a lens plane, as in Ehlers et al (2001); Frittelli & Newman (1999) and Perlick (2004). These works develop a consistent theory of strong lensing entirely on the basis of the null geodesics in an arbitrary spacetime. Image distortion and weak gravitational lensing were considered from this perspective in Frittelli et al. (2001, 2002). An application of this no-lens-plane approach in (non-cosmological) spacetimes representing spherically symmetric non-singular matter distributions is presented in Kling & Newman (1998). The case of Schwarzschild black holes is developed in Frittelli et al. (2001) and the resulting lensing predictions are compared to Virbhadra & Ellis (1999), where a lens-plane approximation is applied to lightrays that undergo large bending. Large bending angles by static and spinning black holes are also treated with an approximation scheme in Bozza et al (2006); Sereno & De Luca (2006), with an application to Sag A*.

The purpose of this paper is to test the accuracy of the conventional approach in determining the total mass of clusters. For this purpose we integrate the null geodesic equations in cosmological lensing spacetimes. We work with actual or realistic strong-lensing scenarios in the standard cosmology, assuming matter distributions of either a three-dimensional singular isothermal sphere (SIS) model or the model of Navarro et al. (1997) (NFW). Both these models are unrealistic to the extent that the mass density does not fall off fast enough to allow for a bounded mass in all space. In principle, some way of truncating the mass density is implicit in the model, although the details of the truncation mechanism are not considered of fundamental relevance to the predicted observables.

Often in the application of gravitational lensing to astrophysical data, truncation is imposed only in the directions transverse to the line of sight. This practice is justified on the basis that the projected mass density required for the thin-lens approximation is actually well defined in the model, as it involves only a one dimensional integration of the mass density along the line of sight, and therefore, truncation of the model along the line of sight is not necessary. Naturally, this practice introduces further error in addition to the error in-

involved in the use of the thin-lens assumption. The accuracy of this conventional model (thin-lens plus lack of truncation along the line of sight) is the issue in our current study.

Our method consists of comparing the observables predicted by the conventional approach to those predicted by the theory with no approximations. The theory is provided by the bending of light in the presence of mass as described by general relativity. The physical scenario common to both problems is the mass-density model. This is used differently in both approaches. In the conventional approach, the mass density is only used after integration along the line of sight, with no truncation. In the relativistic approach, which here we consider to be the exact treatment of the problem, the mass density is used as a source of the Newtonian potential that determines the components of the metric whose null geodesics are sought in exact form. The general relativistic (or exact) approach does not make sense in the absence of truncation along the line of sight. Therefore, our study ends up comparing the results of a non-truncated thin-lens model to a properly truncated general-relativistic numerical integration, both of which represent the same physical situation. For a proper interpretation of our results, it is important to emphasize that the non-truncated thin-lens models are conventionally intended to represent, with some accuracy, the physical situation of a properly truncated mass density, and for this reason the comparison is entirely justified.

Clearly, however, the comparison of the conventional approach with the relativistic treatment provides a measure of the total error incurred by two separate mechanisms: the thin lens approximation, and the lack of proper truncation along the line of sight. The error introduced by the truncation mechanism, or the lack of it, into the thin-lens scheme can be analyzed as an end in itself. In this respect, progress has been made recently in introducing better physical truncation schemes that improve over hard truncation, including Baltz et al (2007) and Takada & Jain (2003). Of importance, Baltz et al (2007) considers differences between truncated and non-truncated lensing observables, giving a measure of the inaccuracy introduced by the truncation mechanism into the thin-lens scheme. These studies take the properly truncated thin-lens scheme

as the exact model of the physical situation, thus they fail to properly account for the actual inaccuracy with respect to the general relativistic theory. The size of the truncation error by itself within the thin-lens scheme has little meaning if the actual error introduced by the thin-lens assumption is not known.

In order to give an idea of the sizes of both errors (thin-lens and lack of truncation) with respect to the relativistic theory, we also compare our integration of the null geodesics with thin-lens models truncated along the line of sight. In this case, the inaccuracy of the model is entirely due to a single assumption: that of thin lenses. Our mechanism of truncation is as simple as possible: a hard cut off of the mass density after an arbitrarily chosen radius.

In Section 2, we outline the ways the Robertson-Walker (RW) background geometry enters our calculation, and in Section 3, we outline the equations of motion. The SIS and NFW gravitational potentials and thin-lens models are developed in section 4. Section 5 describes our experimental set-up, numerical approach, and numerical accuracy. Our main results comparing the accuracy of the thin-lens models are presented in section 7. Section 8 presents the variation of thin-lens accuracy as a function of cosmology parameters for a range of flat cosmologies. We discuss and explain our results in section 9 before concluding with some comments about our results and the their implications for lensing studies in section 10.

2. Cosmological background

We take as the background a flat RW metric with the current accepted values of the Hubble constant $H_0 = 70$ km/s/Mpc, the matter density $\Omega_m = 0.3$ and the cosmological constant density $\Omega_\Lambda = 0.7 = 1 - \Omega_m$. The metric is

$$ds^2 = c^2 dt^2 - a^2(t) \{ dr^2 + r^2(d\theta^2 + \sin^2\theta d\phi^2) \}, \quad (1)$$

with a scale factor $a(t)$ for our cosmological model as in Ryden (2003)

$$a(t) = \left(\frac{\Omega_m}{\Omega_\Lambda} \right)^{1/3} \left\{ \sinh \left(\frac{3H_0\sqrt{\Omega_\Lambda}t}{2} \right) \right\}^{2/3}. \quad (2)$$

The Hubble parameter $H \equiv \dot{a}/a$ is

$$H^2 = H_0^2 \left(\frac{\Omega_m}{a(t)^3} + (1 - \Omega_m) \right). \quad (3)$$

We will be considering photons emitted by a source at emission time t_e , and arriving at the observer at the observation time t_o . For numerical convenience, we fix the scale factor to the value 1 at the observation time, $a(t_o) = 1$, which yields $t_o = 4.248 \times 10^{17}$ s.

A natural way to give the relative locations between the lens, observer, and source is to place the lens at the spatial origin, and to use the redshifts to determine the positioning of the lens and observer. Using the redshift relation, $1 + \tilde{z} = \frac{a(t_o)}{a(t_e)}$, and setting $a(t_o) = 1$, we can solve for the value of t_e with Eq. 2.

To obtain the radial positions of the source and observer, we orient our coordinates in such a way that a light ray travels radially in the background spacetime and assume that the observer, lens and source are at least nearly co-linear. We can then integrate radial null geodesics of the metric Eq. 1 to determine the radial positions of the source and observer (by ignoring the perturbation introduced by the lens).

3. Equations of motion

The lensing scenario is described in terms of the following weakly perturbed RW metric

$$ds^2 = (1 + 2\varphi)dt^2 - a^2(1 - 2\varphi) \times \{ dr^2 + r^2(d\theta^2 + \sin^2\theta d\phi^2) \}, \quad (4)$$

This metric is accurate to first order in φ , which is a Newtonian potential determined by the proper mass density of the lens ρ_p via

$$\nabla_p^2 \varphi = 4\pi G \rho_p, \quad (5)$$

where the derivatives in the Laplacian operator are taken with respect to the proper distance $r_p = a(t)r$. Commonly, the proper mass density is taken as a function $\rho_p(r_p)$ which depends explicitly on the proper distance r_p but not on the time t .

Under conventional lensing conditions, a light-ray spends a very small amount of time in the

area of influence of the lens (where $\varphi \neq 0$). During such a small time the scale factor of the universe $a(t)$ changes very little. It is typically assumed that under such conditions, this scenario is consistent with the Einstein equations for a linearized perturbation off a FRW spacetime. The consistency of a general cosmological lensing scenario with the Einstein equations is studied in Futamase & Sasaki (1989).

By Eq. 5, the potential φ is an explicit function of the proper distance r_p but not the time t . Necessarily, thus, the potential is a function of both the comoving distance r and the coordinate time t via:

$$\varphi = \varphi(r_p) = \varphi(a(t)r) = \varphi(t, r). \quad (6)$$

Consequently, the metric, Eq. 4, is not strictly static in the comoving coordinate system. This issue is somewhat obscure in the standard references, including the excellent books by Schneider et al. (1992) and Petters et al. (2001), where the potential is said to be “time independent.” The time-variation of the potential is small, however, in the conditions of lensing, where the scale factor changes very little during the passage of a lightray (one has $d\varphi/dt = (da/dt) \times (r/a) \times \partial\varphi/\partial r$). So during the passage through the lens one may approximate the scale factor by its value at some time t_l representative of the time at which the lightray passes the lens. This would make the metric around the lens approximately static for the purposes of calculating, for instance, the time delay due to the lens.

For our purposes the metric is needed for the entire trajectory from the source to the lens, along which one expects the scale factor to change perhaps significantly. The metric is not, thus, independent of time, but it is conformal to an approximately time-independent metric. Since the null geodesics of conformally related spacetimes are identical, we may choose to approximate the scale factor with its value at the lens or not. Although the approximation is very valuable for the purpose of obtaining a closed form expression for the lens equation in the conventional approach, it brings no real advantage to the numerical integration of the null geodesics, so we prefer to maintain the time dependence as prescribed by Poisson’s equation. The equations of motion are more com-

plicated (in particular, they do not decouple) but the added complications do not represent a real obstacle.

Since the lens model Eq. 4 is spherically symmetric, the particle trajectories are planar, and there is no loss of generality in choosing the plane as $\theta = \pi/2$. The geodesic equations can be found explicitly as the Euler-Lagrange equations of the Lagrangian

$$\mathcal{L} = (1+2\varphi)\dot{t}^2 - a^2(t)(1-2\varphi)\{\dot{r}^2 + r^2\dot{\phi}^2\} = 0, \quad (7)$$

to first order in φ . The Lagrangian is equal to zero because the geodesics are null.

Since the coordinate ϕ is cyclic, the Euler-Lagrange equations are equivalent to five first-order ODEs, which we can write as

$$\begin{aligned} \dot{t} &= v_t \\ \dot{r} &= v_r \\ \dot{v}_t &= \left(4\varphi \frac{\partial\varphi}{\partial t} - \frac{da}{dt} \frac{1}{a}\right) v_t^2 - 2(1-2\varphi) \frac{\partial\varphi}{\partial r} v_t v_r \\ \dot{v}_r &= -2v_t v_r \left(\frac{da}{dt} \frac{1}{a} - (1+2\varphi) \frac{\partial\varphi}{\partial t}\right) \\ &\quad + 4\frac{\varphi}{a^2} \frac{\partial\varphi}{\partial r} v_t^2 - \frac{2b^2}{a^4 r^2} \frac{\partial\varphi}{\partial r} (1+6\varphi) \\ &\quad + \frac{b^2}{a^4 r^3} (1+4\varphi) \\ \dot{\phi} &= -\frac{b}{a^2 r^2} (1+2\varphi). \end{aligned} \quad (8)$$

These equations are obtained by working to first order in φ and making use of $\mathcal{L} = 0$ in the form

$$a^2(\dot{r}^2 + r^2\dot{\phi}^2) = (1+4\varphi)\dot{t}^2. \quad (9)$$

The parameter b arises from $\ddot{\phi} = 0$ and is related to the “observation angle” at the observer or the angle between the lightray and the optical (radial) axis connecting the observer to the lens. The relationship is determined by taking the dot product of the spatial part of the null vector at the observer with a unit vector pointing towards the origin. Using the spatial part of the metric, Eq. 4, one obtains

$$\sin \theta_{obs} = \theta_{obs} = \frac{b}{r_0} (1+2\varphi_0), \quad (10)$$

where the potential, φ_0 , is evaluated at the observer position at t_0 .

We will be integrating past null geodesics from the observer back to hypothetical sources. Therefore, we need to specify five constants of integration:

$$t_0, r_0, \phi_0, v_{t_0}, v_{r_0}. \quad (11)$$

This is in addition to the constant b which essentially fixes the initial value of $\dot{\phi}_0$. For the initial position (t_0, r_0, ϕ_0) we take $t_0 = 1$ by setting the unit scale to the age of the universe, $\phi_0 = 0$ by arbitrary choice, and set r_0 using the redshift of the lens (which is placed at the origin), as was described in section 2. The initial value of \dot{v}_t is set to -1 , and then by $\mathcal{L} = 0$, we determine the initial value of v_r . Note that by choice of units, we have $a(t_0) = 1$. From Eq. 9 and 8, we have

$$v_{r_0} = -\sqrt{(1 + 4\varphi_0) \times (1 - b^2/r_0^2)}, \quad (12)$$

where $\varphi_0 = \varphi(t = 1, r = r_0)$, and we take the overall minus sign to make the rays approach the lens.

4. SIS and NFW Models

The SIS and NFW matter distributions are simple spherically-symmetric matter models in common use in lensing and other studies. An inconvenience of both these models is that the total mass is unbounded. In this section, we develop the three-dimensional gravitational potentials for these models assuming that the matter extends to some proper radius r_c with zero matter density for $r_p > r_c$. We also develop two-dimensional (projected) thin-lens matter distributions for each model with and without truncation for $r_p > r_c$.

4.1. SIS Newtonian potential

The singular isothermal sphere (SIS) model is appealing because it predicts flat rotation curves. In the SIS model the mass enclosed in a sphere of proper radius r_p is

$$M(r_p) = \frac{2\sigma_v^2 r_p}{G}, \quad (13)$$

where the parameter σ_v is the velocity dispersion, independent of the cluster redshift. For $r_p < r_c$ where r_c is some truncation radius to be determined, the SIS proper mass density ρ_p^{SIS} is given by

$$\rho_p^{SIS} = \frac{\sigma_v^2}{2\pi G r_p^2}. \quad (14)$$

We assume that the matter density of the perturbation vanishes for $r_p > r_c$. Notice that the value of r_c can be chosen independent of redshift, because the SIS mass model contains no redshift dependence. Thus for $r_p > r_c$ the potential is that of a point mass enclosing a mass $M(r_c)$.

The potential for $r_p < r_c$ is the solution of Poisson's equation that matches the point mass potential smoothly (continuously and with continuous first radial derivative) at r_c . We thus have:

$$\varphi(r_p) = \begin{cases} 2\sigma_v^2 \ln x - 2\sigma_v^2 & x < 1 \\ -\frac{2\sigma_v^2}{x} & x > 1 \end{cases}, \quad (15)$$

where $x = r_p/r_c$ is a natural dimensionless radial parameter.

To have the potential in the comoving coordinates, we make the substitution $r_p = a(t)r$ in the potential, Eq. 15. Henceforward, x is to be thought of as $x = \frac{a(t)r}{r_c}$. The three-dimensional SIS model is thus a two-parameter model, depending on σ_v and r_c .

4.2. SIS Thin lenses

In this subsection, we derive the projected mass density and a thin lens equation for the SIS model with a truncation radius, and show how the usual presentation arises as a limiting case in which one of the two parameters is lost.

The projected two-dimensional mass distribution is

$$\Sigma_p^{SIS} = \int_{-z_c}^{z_c} \rho_p^{SIS} dz_p, \quad (16)$$

with ρ_p^{SIS} given by Eq. 14 and where z_p is the proper coordinate along the optical axis. The limit of integration is $z_c = \sqrt{r_c^2 - s^2}$, where s is the proper distance to the optical axis. The integral can be evaluated in closed form, yielding

$$\Sigma_p^{SIS}(s) = \frac{\sigma_v^2}{\pi G s} \arctan \left(\sqrt{\frac{r_c^2}{s^2} - 1} \right). \quad (17)$$

The mass interior to a proper radius s is

$$M(s) = \frac{2\sigma_v^2 s}{G} A(r_c/s) \quad (18)$$

with

$$A(r_c/s) \equiv \arctan \left(\sqrt{\frac{r_c^2}{s^2} - 1} \right) + \frac{r_c}{s} \left(1 - \sqrt{1 - \frac{s^2}{r_c^2}} \right). \quad (19)$$

The bending angle as a function of s is (Schneider et al. 1992)

$$\hat{\alpha} = \frac{4GM(s)}{s}. \quad (20)$$

For a source at position y from the optical axis, the images will be seen on the same line at positions x related to y by the lens equation which, with Eq. 20, takes the form

$$y = \frac{D_s}{D_l} x - 8D_{ls}\sigma_v^2 \frac{x}{|x|} A(|x|/r_c) \quad (21)$$

for angular diameter distances to the source, lens, and between the lens and source, D_s , D_l , and D_{ls} , respectively. The dependence on the truncation radius r_c appears in the factor $A(|x|/r_c)$. In typical lensing situations the impact parameter $|x|$ is much smaller than the truncation radius r_c . The Taylor expansion of $A(|x|/r_c)$ for small ratio $|x|/r_c$ is

$$A(|x|/r_c) = \frac{\pi}{2} - \frac{|x|}{2r_c} - \frac{|x|^3}{24r_c^3} + \dots \quad (22)$$

In practice, it is customary to neglect the dependence on the truncation radius r_c and substitute the factor $A(|x|/r_c)$ by its limiting value $\pi/2$, leading to the standard SIS lens equation found for instance in Schneider et al. (1992). The comparison with conventional results is easier to make by introducing scaled quantities,

$$\bar{y} = \frac{yD_l}{\xi_0 D_s} \quad \& \quad \bar{x} = \frac{x}{\xi_0},$$

with

$$\xi_0 = 4\pi \left(\frac{\sigma_v}{c} \right)^2 \frac{D_l D_{ls}}{D_s}. \quad (23)$$

Using these scaled quantities, the lens equation reads

$$\bar{y} = \bar{x} - \frac{2}{\pi} \frac{\bar{x}}{|\bar{x}|} A(\bar{r}_c/|\bar{x}|), \quad (24)$$

which in the limit of large truncation radius reduces to the conventional form

$$\bar{y} = \bar{x} - \frac{\bar{x}}{|\bar{x}|}. \quad (25)$$

One sees that the thin-lens SIS model really contains two parameters. Under the normal conditions of gravitational lensing this is considered as a one-parameter model, because an assumption has been made on the relative sizes of r_c and x . In the comparisons that follow, we will be making reference to both SIS lens equations: the conventional one-parameter SIS model (Eq. 25), and the two-parameter SIS model (Eq. 24).

We will be interested in the Einstein ring radius, which is given by the value of x satisfying Eq. 21 with $y = 0$. For the conventional one-parameter thin-lens SIS model, the Einstein ring angle $\theta_E^{tl} = x/D_l$ is given by

$$\theta_E^{tl} = 4\pi \frac{\sigma_v^2 D_{ls}}{c^2 D_s}, \quad (26)$$

Technically, this thin lens result assumes that the truncation radius r_c is large compared to the scale radius ξ_0 (Schneider et al. 1992).

In the two-parameter thin-lens SIS model, the Einstein ring angle is given by the root of

$$\theta - 8 \frac{D_{ls}}{D_s} \frac{\sigma_v^2}{c^2} A = 0, \quad (27)$$

where A , by Eq. 19, is

$$A = \arctan \left(\sqrt{\frac{r_c^2}{D_l^2 \theta^2} - 1} \right) + \frac{r_c}{D_l \theta} \left(1 - \sqrt{1 - \frac{D_l^2 \theta^2}{r_c^2}} \right). \quad (28)$$

4.3. NFW Newtonian potential

The matter distribution of the NFW model Navarro et al. (1997) is given by

$$\rho_p = \frac{\delta_c \rho_c r_s^3}{r_p (r_p + r_s)^2}, \quad (29)$$

where $\rho_c = 3H^2(z)/(8\pi G)$ is the critical density of the universe as a function of redshift. The two parameters of the model are the scale radius, r_s , and δ_c . In the literature δ_c is often replaced by the concentration parameter c defined by

$$\delta_c = \frac{200}{3} \frac{c^3}{\ln(1+c) - c/(1+c)}, \quad (30)$$

and the scale radius r_s is replaced by the virial radius $r_{200} = c r_s$, which is the radius inside which the average mass density is $200\rho_c$.

Like the SIS model, the total mass over all space is undefined, so we must truncate the model at some radius r_c . However, because the NFW model is indexed to ρ_c , the mass interior to a constant proper radius varies with redshift.

We choose to hold the mass of the halo constant and truncate the NFW profile at r_{200} , so that the constant total mass of the halo is

$$M_{200} = \frac{800\pi}{3} \rho_c r_{200}^3. \quad (31)$$

The truncation radius $r_c = r_{200}$ is then a known function of redshift through ρ_c :

$$r_{200} = \left(\frac{3 M_{200}}{800\pi \rho_c} \right)^{1/3}. \quad (32)$$

In practice, we pick a value for r_{200} at the time the lightray passes the lens and use Eq. 31 to compute constant halo mass and Eq. 32 to determine the truncation radius as a function of time. For $x \equiv r_p/r_{200} < 1$, the enclosed mass is

$$M = M_{200} \left(\frac{\ln(1+cx) - \frac{cx}{(1+cx)}}{\ln(1+c) - \frac{c}{(1+c)}} \right), \quad (33)$$

where c is the concentration parameter.

The NFW gravitational potential is obtained by smoothly matching the spherically symmetric gravitational potential for the mass density given

by Eq. 29 to a point mass potential at $x = 1$. The result is

$$\varphi = -\frac{G M_{200}}{r_{200}} \begin{cases} \frac{\frac{1}{x} \ln(1+cx) - \frac{c}{1+c}}{\ln(1+c) - \frac{c}{1+c}} & x < 1 \\ \frac{1}{x} & x > 1 \end{cases} \quad (34)$$

where for cosmological spacetimes, we take $x = a(t)r/r_{200}$, with r_{200} defined in Eq. 32 and constant concentration parameter c .

4.4. NFW Thin lenses

We begin our discussion of NFW thin-lens models by determining the two-dimensional, projected mass density used in gravitational lensing with an arbitrary truncation radius r_c . We initially scale by r_s so that $\tilde{r}_p = r_p/r_s$ and use cylindrical coordinates where $\tilde{r}_p = \sqrt{\tilde{x}^2 + \tilde{z}^2}$ where $\tilde{z} = z/r_s$ runs along the optical axis and $\tilde{x} = s/r_s$ is the scaled distance from the z axis. We define $\gamma = r_c/r_s$ to be an arbitrary scaled cutoff radius (we will later set $r_c = r_{200}$).

The surface mass density is then given by

$$\begin{aligned} \Sigma_p^{NFW} &\equiv 2r_s \int_0^{\sqrt{\gamma^2 - \tilde{x}^2}} \rho d\tilde{z} \\ &= 2\delta_c \rho_c r_s \int_0^{\sqrt{\gamma^2 - \tilde{x}^2}} \frac{d\tilde{z}}{\sqrt{\tilde{x}^2 + \tilde{z}^2} (1 + \sqrt{\tilde{x}^2 + \tilde{z}^2})^2}, \end{aligned} \quad (35)$$

and we make the change of variable $\tilde{z} = \tilde{x} \tan u$. Then the closed form expressions for the projected mass density are for $\tilde{x} > 1$,

$$\begin{aligned} \Sigma_p^{NFW} &= 2\delta_c \rho_c r_s \frac{1}{\tilde{x}^2 - 1} \left[\frac{2\tilde{x}Y}{(1 + \tilde{x} + Y^2(\tilde{x} - 1))} \right. \\ &\quad \left. - \frac{2}{\sqrt{\tilde{x}^2 - 1}} \arctan \left(Y \sqrt{\frac{\tilde{x} - 1}{\tilde{x} + 1}} \right) \right], \end{aligned} \quad (36)$$

and for $\tilde{x} < 1$,

$$\begin{aligned} \Sigma_p^{NFW} &= 2\delta_c \rho_c r_s \frac{1}{\tilde{x}^2 - 1} \left[\frac{2\tilde{x}Y}{(1 + \tilde{x} + Y^2(\tilde{x} - 1))} \right. \\ &\quad \left. - \frac{2}{\sqrt{1 - \tilde{x}^2}} \operatorname{arctanh} \left(Y \sqrt{\frac{1 - \tilde{x}}{\tilde{x} + 1}} \right) \right], \end{aligned} \quad (37)$$

and for $\tilde{x} = 1$,

$$\Sigma_p^{NFW} = 2\delta_c \rho_c r_s \frac{Y}{2} \left(1 - \frac{Y^2}{3} \right), \quad (38)$$

where

$$Y \equiv \tan \left[\frac{1}{2} \arctan \sqrt{(\gamma/\tilde{x})^2 - 1} \right]. \quad (39)$$

As $\gamma = r_c/r_s \rightarrow \infty$ we have $Y \rightarrow 1$ and we recover the conventional NFW projected matter density, independent of the truncation radius, Eq (11) in Wright & Brainerd (2000).

In the limit that $\gamma = r_c/r_s \rightarrow \infty$, a closed form expression for the mass interior to a radius ρ can be found and is reported in Wright & Brainerd (2000) and elsewhere. Written in terms of the concentration parameter c and the scaled projected radius in the lens plane $\bar{s} = s/r_{200}$, this closed form expression for the mass is

$$M(s) = \frac{100 r_{200}^3 H^2}{\ln(1+c) - c/(1+c)} Q(\bar{s}), \quad (40)$$

where $Q(\bar{s})$ is given by

$$Q(\bar{s}) = \begin{cases} \frac{2}{\sqrt{1-(c\bar{s})^2}} \operatorname{arctanh} \sqrt{\frac{1-c\bar{s}}{1+c\bar{s}}} + \ln \frac{c\bar{s}}{2} & c\bar{s} < 1 \\ \frac{2}{\sqrt{(c\bar{s})^2-1}} \operatorname{arctan} \sqrt{\frac{c\bar{s}-1}{c\bar{s}+1}} + \ln \frac{c\bar{s}}{2} & c\bar{s} > 1 \end{cases} \quad (41)$$

There is no closed form expression that we are aware of for the mass interior to a radius s in the case of a truncated NFW model. We simply find the mass by numerically integrating Eq. 37. This numerical integration can be carried out using Gauss-Legendre quadratures, since the integrand is regular, or by turning the integral equation into a differential equation and solving with a

numerical ODE solver with adaptive stepsize. In either case, it is critical to sample well the region near $s = 0$ because the integrand has derivatives that are undefined there.

Given the mass within a radius $|x|$, the lens equation

$$y = \frac{D_s}{D_l} x - \frac{4GD_{ls}M(|x|)}{x} \quad (42)$$

is the basis for conventional gravitational lensing by NFW models, in the same way as for the SIS model. The Einstein ring angles will be determined by the roots of Eq. 42 for $y = 0$.

5. Experimental testbed

We maintain the source, lens and observer on the same axis, so that the observer will see Einstein rings around the lens at an angle θ_{obs} in Eq. 10. This observation angle will be considered as a function of the lens model parameters and the relative positioning of the lens, observer and source.

Since the SIS model is a one parameter model (holding fixed the truncation radius r_c), fixing the Einstein ring angle results in a determined value of σ_v . It is fairly common in strong lensing articles to use a simple SIS model in this manner, even when two symmetric arcs are found instead of a ring. While it is known that this method leads to an overestimate of the lens mass, this direct relation between σ_v and the ring angle serves as a good comparison for this paper.

There is a degeneracy in specifying the Einstein ring angle as the only observable for NFW models, since the NFW models contain two parameters. However, weak lensing studies based on gravitational shearing of background images tend to show that the virial radius r_{200} is often better constrained than the concentration parameter c . In addition, weak lensing studies tend to find very little tangential shear, a direct measure of the mass, at physical radii greater 3.5 Mpc. For these reasons, in this paper we will generally specify that $r_{200} = 3.5$ Mpc when the light passes the lens and think of the concentration parameter of the NFW models as the dynamical variable tied to observed Einstein rings. We find that the errors in the thin-lens cited in this paper do not appreciably vary when r_{200} is reset to new values within

an expected r_{200} range.

We consider a number of galaxy clusters with known redshifts as lens candidates. As a benchmark system, we consider RXJ1347-1145, a high X-ray luminosity cluster at $z = 0.45$ that has been widely studied in weak and strong lensing. RXJ1347-1145 has a pair of arcs at redshift 0.8, located at approximated 35 arc sec from the gravitational center of the cluster. We also consider a cluster discovered by Wittman et al. (2003) at $z = 0.68$ that appears to have a pair of arcs at 7 arc sec at an unconfirmed redshift. To consider a range of lens redshifts, we also include Abel 1451 at $z = 0.2$, whose weak lensing signal is reported in Cypriano et al. (2004) and RDCS1252.9-2927, a high redshift cluster ($z = 1.24$) with a weak lensing measurement from HST imaging reported in Lombardi et al. (2005).

We note that the mass density inferred from the weak lensing measurements of these clusters has fallen to essentially zero at a projected radius in the lens plane by approximately 3.5 Mpc. Therefore, in our standard comparisons, we choose the SIS truncation radii of 3.5 Mpc, the same as the NFW cases, although in some comparisons we allow for a range of truncation radii. 3.5 Mpc is generally a factor of 10 to 50 larger than the scale radius, Eq. 23.

6. Numerical approach and accuracy

For the purposes of integrating the null geodesics, we re-scale the time and radial coordinates:

$$t' = \frac{t}{t_o} \quad r' = \frac{r}{ct_o}. \quad (43)$$

In the t' coordinate, the observer receives the light rays $t' = 1$, and the metric is rescaled by an overall factor

$$ds^2 = (ct_o)^2 \left(dt'^2 - a^2(t') \times \{ dr'^2 + r'^2(d\theta^2 + \sin^2\theta d\phi^2) \} \right), \quad (44)$$

which, of course, does not alter the null geodesics.

We use a ray shooting technique to determine the observation angle for a given positioning and set of lens model parameters. For example, if the Einstein ring angle is fixed, increasing σ_v or c will

cause the true light ray to cross the optical axis closer to the lens. This allows us to vary one model parameter at a time for a given Einstein ring angle, using Newton's method to determine the parameter value to a high accuracy, limited essentially by the quality of the ODE integration scheme.

We integrate the null geodesic equations using an adaptive stepsize Runge-Kutta-Fehlberg 4-5 method based on the implementation in Press et al. (1995). This allows us to monitor the error in each step and maintain a known, and small, accumulated error in the integration. We purposefully slow the integration (over the affine parameter) as we approach the source location, where the adaptive stepsize algorithm would naturally take large steps, in order to carefully stop at the source position.

The principal source of error in our method is in stopping at the source position. With the observer at $\phi = 0$ and source at ϕ_f , we integrate over the affine parameter until $\phi = \phi_f \pm \epsilon_\phi$ and determine whether $r = r_l \pm \epsilon_r$ where r_l is the known lens position. Based on whether r is less than or greater than r_l , we accept or change initial values at the observer. In practice, we find that the error introduced by this stopping condition is orders of magnitude greater than the error accumulated in the ODE integration. In the materials below, the error bars on the numerical integration are derived from this known error source.

We consider results from the numerical integration of the null geodesic equations, Eq. 8, to be the "correct" results from lensing which we compare the thin-lens models to. As an estimate of the error in our ODE integration, we first set the Einstein ring angle to known value, θ_E , and solve for the parameter value (either σ_v or c). We then solve backwards for the Einstein ring angle our numerical integration predicts given these parameter values, and subtract from the original specified angle.

The difference, which should be zero, is an estimate of the error our methods allow. Figure 1 shows this error estimate for a SIS model of RXJ1347-1145, a cluster at $z = 0.45$ with arcs from a $z = 0.8$ source. The error values are all small and show relatively little trend. Similar results are obtained in the NFW models.

By contrast, when one specifies the Einstein

ring angle, solves the geodesic equations to determine the model parameters, then asks for the value of the ring angle predicted by the thin-lens model for those parameters, one sees a significant difference from the original angle. Figure 2 shows the error, $\Delta\theta_E = \theta_E - \theta_E^{tl}$, in the Einstein ring angle predicted by the thin-lens methods for a SIS model to be much larger than the numerical scatter for RXJ1347-1145.

Using the error introduced by the stopping conditions to form error bars, we show the difference between the predicted velocity dispersion for a given angle in a SIS model in Fig. 3 for a RXJ1347-1145 setup with $r_c = 3.5$ Mpc. The error bars are drawn 1000 times larger than the actual error.

These error estimates and plots with error bars confirm that the differences measured between values predicted by the numerical integration of the geodesic equations and the values predicted by the various thin-lens models are not attributable to truncation or roundoff error in the numerical code.

7. Thin-lens accuracy

Since we are primarily interested in the error introduced in the thin-lens approximation in predicting the mass of the cluster, we cite the relative error in the square of the velocity dispersion,

$$\frac{\Delta\sigma_v^2}{\sigma_v^2} = \frac{\sigma_v^2 - \sigma_v^{tl^2}}{\sigma_v^2}, \quad (45)$$

for SIS models, and the relative error in c ,

$$\frac{\Delta c}{c} = \frac{c - c^{tl}}{c}, \quad (46)$$

for NFW models. The SIS error is equal to the fractional error in the predicted mass. However, due to the differences in the NFW 3-d enclosed mass and conventional enclosed masses, it is more difficult to think of errors in c translated to errors in mass for NFW models.

As a first comparison, we consider a lens and source for RXJ1347-1145 (source at $z = 0.8$) and RDCS1252.9-2927, where we assume a source is located at $z = 1.5$ on the optical axis, and compute the velocity dispersion for a given observed Einstein ring angle using the non-perturbative method and the two thin lens methods. Figure

4 shows the relative error in the square of the velocity dispersion as a function of the observed Einstein ring angle for a cutoff radius of 3.5 Mpc. We see that the errors tend to approach 1% for physical values for the conventional one-parameter SIS thin-lens. The truncated SIS thin lens models tend to perform better, with approximately one fourth the fractional error in the total cluster mass.

For the same lens and source combinations, Fig. 5 shows the relative error in c for an NFW model given the Einstein ring angle. Here we assume that $r_{200} = 3.5$ Mpc when the light ray passes the lens, which is the best fit scale radius for RXJ1347-1145 for weak lensing analysis from Kling et al (2005). We see that the error is on the same order of magnitude as the error in the SIS mass prediction for arcs at large observation angles. For small observation angles, there is a significant difference between the values for c predicted by the non-perturbative and thin lens models, but these observation angles are unlikely, because they involve low concentration parameters ($c < 1.0$). The truncated thin-lens NFW models again perform better for physical systems than the conventional thin-lens models, but the error remains on the same order of magnitude.

In Fig. 6, we show how the relative error in the square of the velocity dispersion depends on the cutoff radius for conventional and truncated SIS models, respectively. Here, we consider RXJ1347-1145, and the three curves represent Einstein rings observed at 5, 15, and 35 arc sec. We see that the relative error introduced by using a thin-lens model does depend on the choice of truncation radius and does not go to zero with larger radius.

For NFW models, variation in r_{200} at the time the light ray passes the lens leads to minor changes in the value of c , but not significant changes in the error estimates. For example, weak lensing measurements found the best fit parameters for RXJ1347-1145 to be $r_{200} = 3.5_{-0.2}^{+0.8}$ Mpc (Kling et al 2005). For the physical arcs in this system at 35 arc sec, Table 1 indicates that the fractional errors maintain the same order of magnitude as r_{200} is varied.

Table 2 gives the relative error in mass (or square velocity dispersion) for thin-lens SIS models for four possible scenarios at increasing lens redshift, all with truncation radii of 3.5 Mpc. In all four cases the lens and the source are at fixed

resfhit, and the Einstein ring angle is varied. A number of observations can be made. First, the error in the prediction of the mass incurred by the use of the thin lens approximation alone varies between 0.03% for small rings and 0.3% for large rings. Secondly, the error in the mass incurred by the combination of the thin lens approximation and the removal of truncation varies between 0.1% for small rings and 2% for large rings. Subtracting both errors yields an estimate of the error introduced by the removal of truncation in the thin lens model. One can see that the removal of truncation along the line of sight introduces an error between 5 and 12 times as large as the thin lens assumption does, for small and large rings respectively.

Similarly, Table 3 gives the relative error in c for NFW models where the truncation radius is set to $r_{200} = 3.5$ Mpc when the light ray passes the lens. The scenarios are the same as for Table 2. One can see that the thin lens approximation alone introduces an error in c between 0.3% and 2% in cases of lens redshift less than 1. Perhaps unexpectedly, the conventional approach shows a relative error around 1% to 2% due to the combination of the thin lens assumption and removal of truncation. The truncation alone introduces an error between 1 and 5 times that incurred by the thin lens assumption.

8. Cosmology Dependence

For a given lens and source distance, and a specified observation angle, the values of parameters in a matter distribution model will depend on the assumed cosmological parameters. In this section, we briefly show that while the values of the parameters vary with choice of cosmology, the overall fractional uncertainty in those parameters does not show significant variation.

In particular, because the NFW model is indexed to the critical density as a function of redshift, one might worry that variation in cosmology will have a strong effect on the accuracy of NFW model parameters.

As a simple test case, we present two tables that show the relative errors associated with SIS and NFW model parameters for the physical arcs appearing at 35 arc sec in RXJ1347-1145 as a function of cosmology. While we only consider flat cosmological models, we do consider a wide range in

the matter density Ω_m .

Tables 4 and 5 present the relative errors in σ_v^2 and c respectively for a cutoff radius of 3.5 Mpc. For the NFW model, r_{200} is set to the cutoff radius as before. Both tables show that the accuracy of thin lens models changes only by a factor of 3 or so over a very wide range in flat cosmologies.

9. Discussion

Figure 2 shows comparisons of predicted Einstein ring angles by conventional approaches and by properly truncated thin-lenses, compared to the relativistic prediction by numerical integration. One can see that given a fixed lens mass and distances to the lens and source, just the use of a thin-lens approximation results in a smaller Einstein ring angle for the same truncated mass model. From this, as well as from Tables 2 and 3, we conclude that the use of the thin-lens assumption alone leads to an overestimate of the mass, at least in the case of the two spherically symmetric models that we use.

In calculating the total bending angle accumulated along a photon path, the thin-lens assumption leads directly to the substitution of an undeflected path for the actual photon path, which, being curved, is normally longer than the undeflected path. In all models where the bending increases monotonically along the path, this procedure naturally leads to an underestimate of the total bending, as the integration takes place over a shorter interval. To compensate for the underestimate of bending, the thin-lens assumption overestimates the mass.

In the conventional SIS model, setting the value of σ_v the same as the value in the truncated models essentially means that the conventional model contains more mass: see Eq. 18. With more mass, the Einstein ring angle grows, so the conventional Einstein ring angles in Fig. 2 are larger than the correct angles.

Figures 3 and 4 indicate that for the same observation angles and source and lens positions, the inferred velocity dispersion for a truncated thin-lens model overestimates the true velocity dispersion. Since at the same mass, the truncated thin-lens predicts a smaller angle, increasing the angle to align with the true observation angle increases the mass of the lens, and hence the velocity dis-

persion.

The conventional SIS can achieve this extra mass either by increasing the velocity dispersion or by adding mass along the line of sight past the truncation radius. This second method can, in fact, drive down the velocity dispersion. In Fig. 4, we see a lower velocity dispersion for the conventional model because the extra mass has been stored along the line of sight. For other lens-source-ring angle configurations, plots similar to Fig. 4 show negative dips in the non-truncated square velocity dispersion error at small observation angles, which implies that the conventional SIS model has a higher than correct velocity dispersion.

The relative error in the concentration parameter of NFW models, Fig. 5, shows a similar effect. Increasing the concentration parameter makes the core of the NFW profile steeper, placing more mass towards the center of the distribution. For the truncated NFW thin lens, increasing the concentration parameter increases the central mass to compensate for a required increased bending angle in the same way it did in the SIS case. For the conventional NFW model, the trade-off between extra stored mass along the line of sight and increasing the steepness of the profile results in a shift in the sign of the relative error in c .

10. Conclusion

The principal finding of this paper is that, in the context of the current generation of precision cosmology experiments, the use of the conventional approach in strong gravitational lensing is justified. Our figures and tables demonstrate that in a wide variety of strong lensing scenarios, and for two widely used mass models, the conventional approach works well in predicting cluster masses. Except in cases where the truncation radius is on the order of 1 to 2 Mpc, the errors in the SIS predicted mass are generally less than 2%. The error in concentration parameter for the NFW model is also small except for very high redshift clusters. This shows that concerns over the possibility of artificially high estimates of dark matter content in clusters as a result of the use of the thin-lens approximation are generally unfounded.

For the first time, to our knowledge, we have been able to show that the thin lens assumption

and the removal of the truncation radius along the line of sight contribute to the error in very different measures. Interestingly, the two approximations introduce errors in opposite directions: the thin-lens assumption underestimates the mass, whereas the removal of the truncation radius overestimates it. The error introduced by removing the truncation along the line of sight is of the same order of magnitude as that of the thin-lens assumption in the best case, and up to an order of magnitude larger in the worst case within our study. The truncation error is thus the dominant source of error in the conventional approach. This is a strong indication that, as precision increases in strong lensing observations, in order to gain a significant increase in accuracy it will be necessary, and perhaps even sufficient at first, simply to recover the truncation radius as an additional parameter in thin-lens models.

Truncation issues aside, we find that the error introduced by the thin lens assumption alone for a given truncation method (in our case, hard truncation) varies between 0.03% and 0.3% in the SIS case, and between 0.3% and 2% in the NFW case for lenses at redshift less than 1. Knowledge of the size of this error should be taken into account when considering additional approximations such as proper truncation methods. Errors of this size may become significant in the next 20 years as the observational precision increases.

Perhaps more important than the specific strong lensing finding in this paper is the possible implication of this finding for weak lensing surveys of galaxy clusters. Strong lensing depends on the first derivative of the gravitational potential (the Christoffel symbols of the underlying metric), but weak lensing depends on the second derivative (the curvature). One may advance the conjecture that the higher order (derivative) measurements of weak lensing might be less sensitive to the thin-lens approximation, and therefore more accurate in the determination of the cluster mass.

At the time at which the fundamental parameters are known to 1% or better, this paper develops the appropriate steps for pursuing strong gravitational lensing without lens planes. In particular, we have demonstrated gravitational lensing by weak gravitational potentials in the appropriate cosmological backgrounds by numerical integration of the null geodesic equations of general

relativity to be a feasible task.

A long-standing argument for the use of the thin-lens approximation and against integrating the null geodesic equations has always been the high computational cost of numerical integration compared with the low cost of the (essentially algebraic) thin-lens approach. Ten years ago this was essentially true. However, the current speed and memory capacity of even small workstations removes this argument against using the general relativistic equations instead of the thin-lens method or other higher order approximations such as those proposed by Pyne & Birkenshaw (1993) or Kling et al (2000).

This material is based upon work supported by the National Science Foundation under Grant Nos. PHY-0244752 and PHY-0555218, and a Bridgewater State College Faculty and Librarian Research Grant. We gratefully acknowledge the hospitality and support of the American Institute of Mathematics during the progress of the workshop “Gravitational Lensing in the Kerr Geometry,” AIM, Palo Alto, July 5-10, 2005.

REFERENCES

- Navarro, J. F., Frenk, C. S. & White, S. D.M., 1997, ApJ, 490, 493
- Pyne, T. & Birkinshaw, M., 1993, ApJ, 415, 459
- Kling, T.P., Perez, A., & Newman, E.T., 2000, Phys. Rev. D, 61, 104007
- Kling, T.P., Perez, A., & Newman, E.T., 2000, Phys. Rev. D, 62, 024025
- Ehlers, J., Frittelli, S. and Newman, E.T., *Gravitational Lensing from a Space-Time Perspective*, Boston Studies in the Philosophy of Science: *Festschrift for John Stachel*, edited by J. Renn (Kluwer Academic, Dordrecht, 2001)
- Futamase, T. & Sasaki, M., 1989, Phys. Rev. D, 40, 2502
- Perlick, V., Living Rev. Relativity 7, 9. <http://www.livingreviews.org/lrr-2004-9> cited on October 30, 2018
- Kling, T.P. & Newman, E.T., 1998, Phys. Rev. D, 59, 124001
- Frittelli, S., & Newman, E.T., 1999, Phys. Rev. D, 59, 124001
- Frittelli, S., Kling, T.P., & Newman, E.T., 2001, Phys. Rev. D, 63, 023006
- Frittelli, S., Kling, T.P., & Newman, E.T., 2001, Phys. Rev. D, 63, 023007
- Frittelli, S., Kling, T.P., & Newman, E.T., 2002, Phys. Rev. D, 65, 123007
- Virbhadra, K.S. & Ellis, G.F.R., 1999 A&A, 15, 4
- Bozza, V. et al., 2006, Phys. Rev. D, 73, 063001
- Sereno, M. & De Luca, F., 2006, Phys. Rev. D, 73, 103004
- Baltz, E. et al., 2007, from arXiv:astro-ph:0705.0682.v2
- Takada, M. & Jain, B., 2003, MNRAS, 340, 580
- Ryden, B. *Introduction to Cosmology* (Addison Wesley, New York, 2003)
- Sahu, K. et al., 1998, ApJ, 492, L125
- Kling, T.P. et al., 2005, ApJ, 624, 2
- Schneider, P., Ehlers, J. & Falco, E.E., *Gravitational Lenses*, (Springer-Verlag, Berlin, Heidelberg, 1992)
- Petters, A.O., Levine, H. and Wambsganss, J. *Singularity Theory and Gravitational Lensing*, (Birkhauser, Boston, Basel, Berlin, 2001)
- Press, W.H. et al., 1995, *Numerical Recipes*, Cambridge University Press
- Wright, C.O. & Brainerd, T.G., 2000, ApJ, 534, 34W
- Wittman, D. et al., 2003, ApJ, 517, 218W
- Cypriano, E. et al., 2004, ApJ, 613, 95
- Lombardi, M. et al., 2005, ApJ, 623, 42

r_{200} (Mpc)	c	δ
3.3	4.9	-0.003
3.5	4.3	-0.004
4.3	2.8	-0.006

Table 1: Relative error in c in NFW thin-lens models with a truncation radius for three different values of r_{200} as the light ray passes the lens for the 35 arc sec arcs of.

System	θ_E	σ_v	δ_1	δ_2	δ_3	$\delta_3/ \delta_2 $	
Abel 1451	5	495.5	0.0012	-0.00028	0.0015	5	
	10	701.1	0.0026	-0.00045	0.0031	7	
	15	859.3	0.0039	-0.00059	0.0044	8	
	$z_l = 0.2$	25	1111	0.0067	-0.00083	0.0075	9
	$z_s = 0.8$	35	1316	0.0095	-0.001	0.012	11
RXJ1347-1145	5	674.3	0.0022	-0.00043	0.0026	6	
	10	954.7	0.0045	-0.00069	0.0052	8	
	15	1171	0.007	-0.0009	0.0079	9	
	$z_l = 0.45$	25	1515	0.012	-0.0012	0.0013	11
	$z_s = 0.8$	35	1797	0.017	-0.0015	0.019	12
(Wittman)	5	818.7	0.0026	-0.0006	0.0032	5	
	10	1160	0.0055	-0.00095	0.0064	7	
	15	1422	0.0084	-0.0012	0.0096	8	
	$z_l = 0.68$	25	1842	0.014	-0.0017	0.016	9
	$z_s = 1$	35	2186	0.02	-0.0021	0.022	11
RDCS 1252.9-292	2	767.1	0.00086	-0.00066	0.0015	2	
	4	1086	0.002	-0.0011	0.0031	3	
	7	1437	0.0037	-0.0016	0.0053	3	
	$z_l = 1.24$	10	1719	0.0056	-0.002	0.0076	4
	$z_s = 1.5$	15	2109	0.0088	-0.0026	0.011	4

Table 2: Relative error in the predicted square velocity dispersion for an SIS model with hard truncation at 3.5 Mpc. The hypothetical Einstein ring angles are given in arc sec, and the velocity dispersions are given in km s^{-1} . RXJ1347-1145 has arcs at approximately 35 arc sec, while Wittman has arcs at 7 arc sec. The column headed by δ_1 shows the error in the prediction of c by the model with no truncation radius along the line of sight. Column δ_2 is the error by the model with hard truncation, and represents the error introduced by the thin-lens approximation alone. The difference $\delta_3 \equiv \delta_1 - \delta_2$ represents the error introduced by the removal of the truncation radius. The last column to the right indicates the size of the truncation error compared to the size of the thin-lens error.

System	θ_E	c	δ_1	δ_2	δ_3	$\delta_3/ \delta_2 $	
Abel 1451	5	1.992	0.0043	-0.019	0.023	1	
	10	2.447	0.0084	-0.0096	0.018	2	
	20	3.136	0.0095	-0.0052	0.015	3	
	$z_l = 0.2$	30	3.759	0.0096	-0.0038	0.013	4
	$z_s = 0.8$	40	4.392	0.0094	-0.0032	0.013	4
RXJ1347-1145	5	1.744	0.014	-0.017	0.032	2	
	10	2.234	0.016	-0.0088	0.025	3	
	20	3.048	0.015	-0.005	0.02	4	
	$z_l = 0.45$	30	3.879	0.014	-0.0038	0.018	5
	$z_s = 0.8$	40	4.843	0.014	-0.0033	0.017	5
(Wittman)	5	1.64	0.017	-0.019	0.036	2	
	10	2.145	0.018	-0.01	0.028	3	
	20	3.018	0.017	-0.0058	0.023	4	
	$z_l = 0.68$	30	3.964	0.016	-0.0046	0.021	4
	$z_s = 1$	40	5.138	0.015	-0.0042	0.019	5
RDCS 1252.9-292	2	1.175	-0.022	-0.078	0.056	1	
	4	1.515	0.002	-0.039	0.041	1	
	7	1.883	0.0099	-0.023	0.033	1	
	$z_l = 1.24$	10	2.198	0.012	-0.01	0.029	2
	$z_s = 1.5$	15	2.691	0.013	-0.012	0.025	2

Table 3: Relative error in the concentration parameter, c , for an NFW model. The truncation radius is set to the co-moving physical distance value of $r_{200} = 3.5$ Mpc at the lens crossing time and then varies to maintain a constant mass. The hypothetical Einstein ring angles are given in arc sec. RXJ1347-1145 has arcs at approximately 35 arc sec, while Wittman has arcs at 7 arc sec. The column headed by δ_1 shows the error in the prediction of c by the model with no truncation radius along the line of sight. Column δ_2 is the error by the model with hard truncation, and represents the error intruded by the thin-lens approximation alone. The difference $\delta_3 \equiv \delta_1 - \delta_2$ represents the error introduced by the removal of the truncation radius. The last column to the right indicates the size of the truncation error compared to the size of the thin-lens error.

Ω_m	Ω_Λ	σ_v (km s $^{-1}$)	δ_1	δ_2
0.05	0.95	1708	0.019	-0.0013
0.15	0.85	1750	0.018	-0.0014
0.30	0.70	1797	0.017	-0.0015
0.45	0.55	1833	0.016	-0.0016
0.60	0.40	1862	0.015	-0.0017
0.95	0.05	1913	0.014	-0.0018

Table 4: Relative error in the SIS predicted mass or σ_v^2 , for a SIS model thin lens without (δ_1) and with (δ_2) a cutoff radius of 3.5 Mpc for the physical arcs of RXJ1347-1145 (at 35 arc sec) for various flat cosmologies.

Ω_m	Ω_Λ	c	δ_1	δ_2
0.05	0.95	6.11	0.01	-0.0023
0.15	0.85	5.25	0.012	-0.0028
0.3	0.7	4.34	0.014	-0.0035
0.45	0.55	3.7	0.017	-0.0044
0.6	0.4	3.22	0.02	-0.0053
0.95	0.05	2.46	0.027	-0.0079

Table 5: Relative error in the NFW predicted concentration parameter, for an NFW model thin lens without (δ_1) and with (δ_2) a cutoff radius for various flat cosmologies. The cutoff radius is set to the co-moving physical distance value of $r_{200} = 3.5$ Mpc at the lens crossing time and then varies to maintain a constant mass.

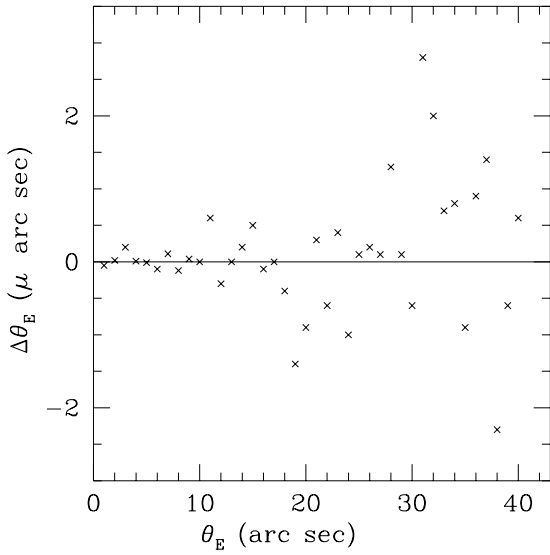


Fig. 1.— A plot estimating the numerical error introduced by integrating the null geodesics and using ray shooting to determine the velocity dispersion (SIS model) or Einstein ring angle. We assume a three-dimensional SIS lens with matter extending to a co-moving radius of 3.5 Mpc lying at $z = 0.45$ and a source at $z = 0.8$. The Einstein ring angle is set, then the velocity dispersion is determined. From this velocity dispersion, we recalculate the Einstein ring angle and subtract from the original angle. These differences are all close to zero and show no trend.

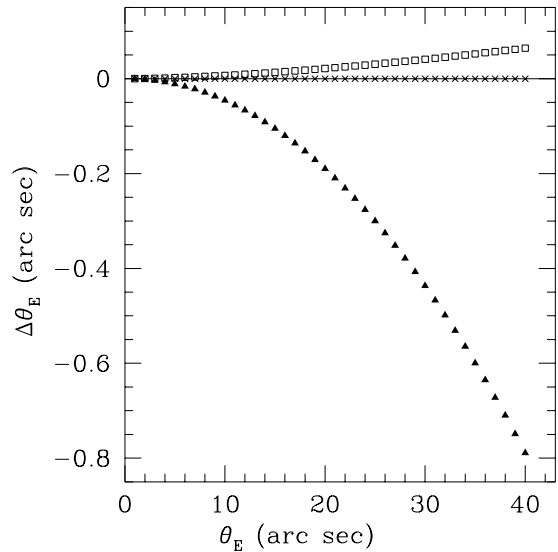


Fig. 2.— A plot showing the numerical scatter of Fig. 1 (crosses) and differences between actual and thin-lens predicted Einstein ring angles for SIS models with (boxes) and without (triangles) a cutoff radius for a lens and source at $z = 0.45$ and 0.8 respectively. A cutoff radius of 3.5 Mpc is used.

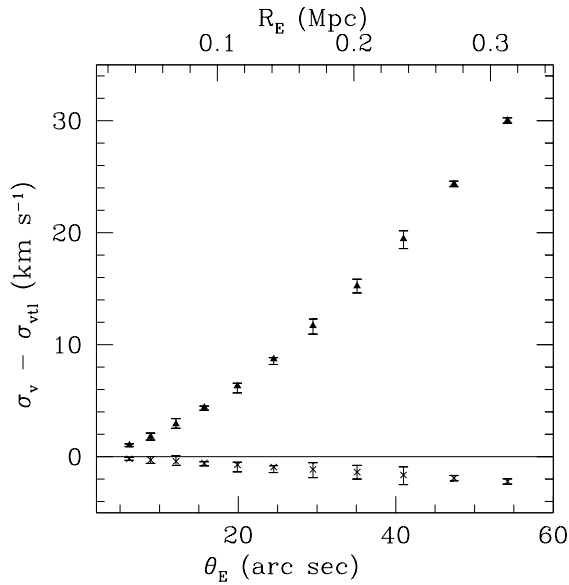


Fig. 3.— A plot of the error in the velocity dispersion introduced by two thin-lens models for arcs of a three-dimensional SIS whose matter extends to a co-moving radius of 3.5 Mpc. The error bars here are drawn 1000 times larger than the actual error bars and reflects an overestimate of the accumulated error in the numerical integration. The triangles correspond to the usual thin-lens SIS model, and the crosses correspond to a thin-lens SIS model that accounts for the finite radius.

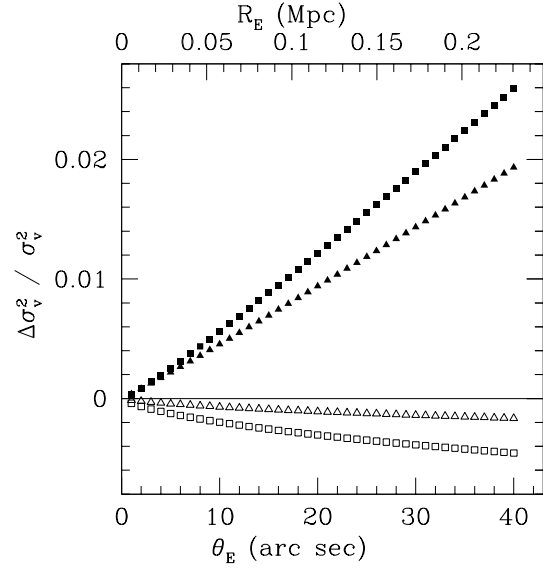


Fig. 4.— A plot of the relative error in the square of the velocity dispersion for an SIS model as a function of the observed Einstein ring angle. The triangles and squares correspond to lens / source redshifts of (0.45, 0.8) and (1.24, 1.5) respectively. The open symbols are the relative error in the SIS model with a cutoff radius, and the closed symbols show the error with no cutoff radius. The cutoff radius used is 3.5 Mpc. The Mpc scale corresponds to the projected Einstein ring radius for a lens at 0.45; the projected radius for a lens at 1.24 would be larger.

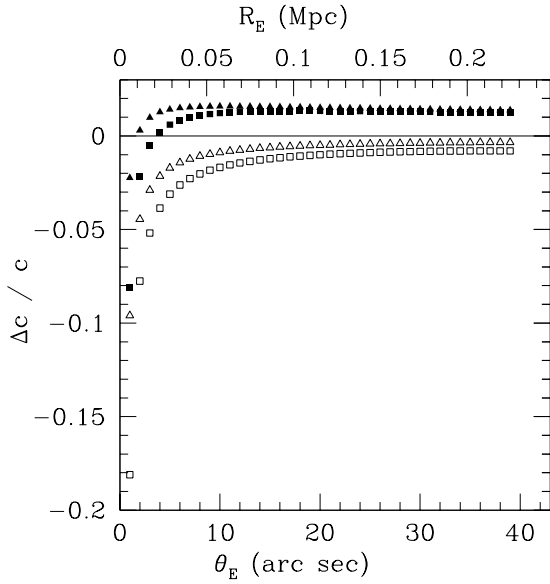


Fig. 5.— A plot of the relative error in c for an NFW model as a function of the observed Einstein ring angle. The triangles and squares correspond to lens / source redshifts of (0.45, 0.8) and (1.24, 1.5) respectively. The open symbols are the relative error in the NFW model with a cutoff radius, and the closed symbols show the error with no cutoff radius. The cutoff radius used is set to the virial radius (r_{200}) as 3.5 Mpc at the lens crossing time and then varies to maintain a constant halo mass. The Mpc scale corresponds to the projected Einstein ring radius for a lens at 0.45; the projected radius for a lens at 1.24 would be larger.

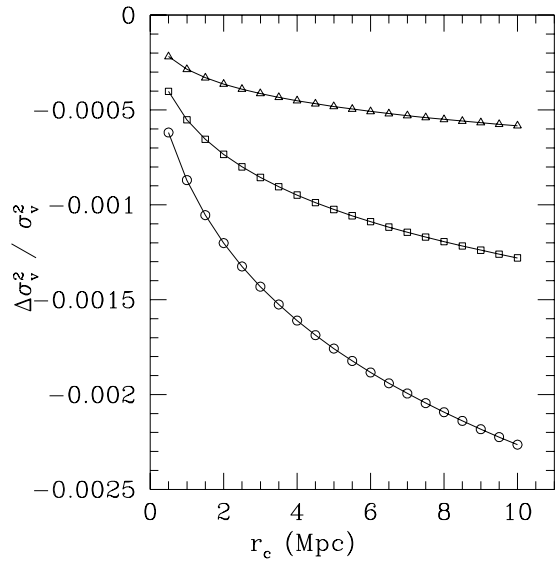


Fig. 6.— A plot of the relative error in the square of the velocity dispersion for thin lens, SIS with a cutoff radius as a function of the cutoff radius. The three curves correspond to errors if the Einstein ring angle is 5 (triangles), 15 (squares) or 35 (circles) arc sec. Here we are considering lensing by RXJ1347-1145, which does have arcs at 35 arc sec.